Determination of low latitude plasma drift speeds from FUV images

Thomas J. Immel, Stephen B. Mende, Harald U. Frey, Laura M. Peticolas

Space Sciences Laboratory, University of California, Berkeley

Eiichi Sagawa

Communications Research Laboratory, Tokyo, Japan

Abstract.
Thousands of images of the nighttime equatorial airglow arcs have been obtained by the far-ultraviolet imager (FUV) on-board the NASA IMAGE satellite. Imaging periods lasting several hours around the time of satellite apogee allow for the determination of the velocity of drifting plasma density depletions occurring within the airglow arcs. These velocities reflect the ExB drift of low-latitude plasma under the influence of a vertical electric field. A survey of several weeks of data produces information regarding the range of electric field magnitudes. Previous results from the Jicamarca radar compare well, validating the this technique as a means of deriving equatorial plasma drift speeds from space.

1. Introduction

The terrestrial equatorial airglow arcs, like the auroral ovals, are persistent features of Earth's far-ultraviolet (FUV) signature [*Carruthers and Page*, 1976]. The arcs appear as a pair of emission bands on either side of Earth's magnetic equator, extending from the dusk terminator eastward across the nightside. Unlike the aurora, their intensity does not indicate the strength or rate of coupling to the magnetosphere, but rather the state of the equatorial ionosphere [*Sojka*, 1991]. The arcs indicate regions of enhanced ionospheric densities where ionospheric plasma is concentrated after rising from the magnetic equator under the influence of daytime dynamo electric fields. The concentration occurs as the plasma diffuses along magnetic field lines which, to the north and south of the magnetic equator, direct the plasma downward into regions of higher plasma densities [*Hanson and Moffett*, 1966]. Due to the complex interaction of the ionosphere and thermosphere in the low-latitude evening sector, localized instabilities can rapidly grow in altitude, resulting in strong localized depletions in plasma densities, with corresponding decreases in airglow brightness in the airglow arcs [*Weber et al.*, 1978]. From years of observations by radars based at low latitudes come the terms "spread-F" to describe the conditions of the destabilized F-region, and "bubbles" or "plumes" to describe the ionospheric depletion associated with the fully developed spatial instability, which is the cause of the large-scale airglow depletions [*Kelley*, 1989].

New global scale studies of these phenomena are now possible using the spectrographic imaging component of the Far Ultraviolet Imager on the IMAGE satellite [*Burch*, 2000; *Mende et al.*, 2000a]. In this study the SI-13 channel is used, which, with its 5-nm passband centered at 135.6 nm, is specifically designed for observations of that emission of atomic oxygen [*Mende et al.*, 2000b]. For auroral or dayside studies, care must be taken to interpret the images with the knowledge that particular emissions of the Lyman Birge Hopfield bands of N_2 also lie in the imager's passband. Since the molecular emission is only produced by direct impact of $\sim$10 eV electrons on N_2, either photoelectrons or secondary auroral electrons, it does not contribute to the SI-13 signal during observations of low latitudes on the nightside.

2. IMAGE Observations

The IMAGE satellite was placed in a highly elliptical orbit (perigee altitude=1000 km, apogee altitude=7.2

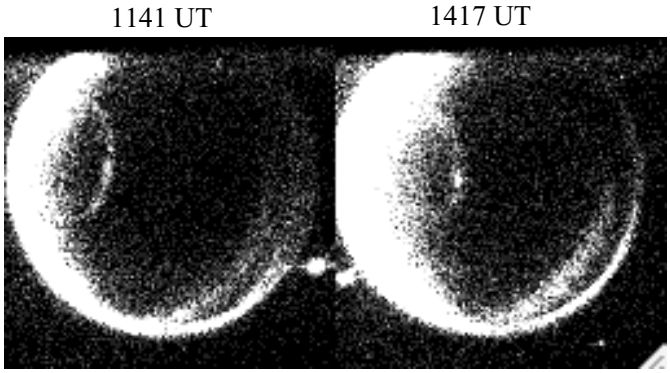

Figure 1. A pair of 135.6-nm images of Earth obtained by the SI-13 instrument on March 28, 2002 (day 87) at 1141 and 1417 UT.

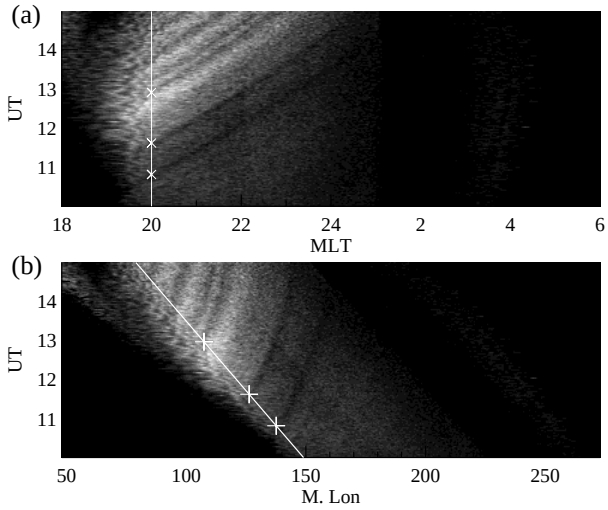

Figure 2. Magnetic Local Time and Longitude keograms of Day 87, 2002, SI-13 imaging period. (a) MLT-UT keogram, showing advance of 135.6-nm O I brightness depressions in local time. (b) Mag. Longitude-UT keogram, showing advance of brightness depressions in magnetic longitude. In each plot the 20 MLT location is indicated with a solid line, on which the crossing times of 3 significant depletions is marked.

R_E) in March of 2000. Apsidal motion of the orbit has caused the latitude of apogee to proceed from 40° to 90° and back down to cross the equator in early 2003. In March, 2002, the latitude was sufficiently low to consistently view the northern airglow arc, with improved viewing of the southern anomaly by May. It is during these months when the local time of apogee is in the evening sector, providing a clear view of the airglow arc from the evening terminator to post-midnight local times. The FUV imaging cadence matches the rotation rate of the satellite which is 2 minutes, with 5 seconds of integration time per SI-13 image.

Two imaging examples are provided in Figure 1, obtained at 1141 and 1417 UT on Day 87 (March 28), 2002. Though the latitude of the satellite moves from 53.7° to 64.9°, the northern airglow arc remains visible. Furthermore, the arc brightens over the time period, with brightnesses $>$ 300 Rayleigh (R) extending to the midnight sector and over a broader range of magnetic latitude. The conversion to brightness from instrument counts is performed according to the UV stellar calibration of the instrument described by *Frey et al.* [2003].

3. Analysis Technique.

Full time series of images must be examined to determine the development of spatial and temporal variations in the arc's brightness. To do this, the images are re-mapped to a regularly spaced grid of magnetic local time (MLT) and latitude (Mag. Lat.), and the instrument counts between 0 and 30° Mag. Lat. are added to report a single number for each 0.5° increment of MLT [see also *Sagawa et al.*, 2003, for further use of this technique]. Processing all available images for an imaging pass results in a data set which can be presented as a keogram, with UT on the vertical axis and MLT on the horizontal axis. The keogram reveals the relative MLT motion of brightness irregularities as a function of UT. For this and all further work, the APEX magnetic coordinate system is used [*Richmond*, 1995].

The MLT-UT keogram for the imaging period including the images of Figure 1 is shown in Figure 2a. The decreases in total 135.6-nm emission intensity in the airglow arc is revealed in this presentation by the several dark tracks which advance in MLT as a function of UT. The apparent motion of the brightness decreases in MLT is obvious, and the keogram clearly shows the development of 5 patches which cross the MLT=20 hours sector at 1050, 1140, 1255, 1310, and 1340 UT. There is also a traveling enhancement in brightness which crosses MLT=20 around 1230. In terms of development of spread-F in the evening sector, this is an active period with instabilities growing into multiple large plumes in $<$ 4 hours time.

The data from the same imaging period are replotted in a co-rotating frame in Figure 2b. The horizontal axis now shows the magnetic longitude (Mag. Lon.) of the FUV measurements during the same time period as in Figure 2a. Features fixed with respect to locations

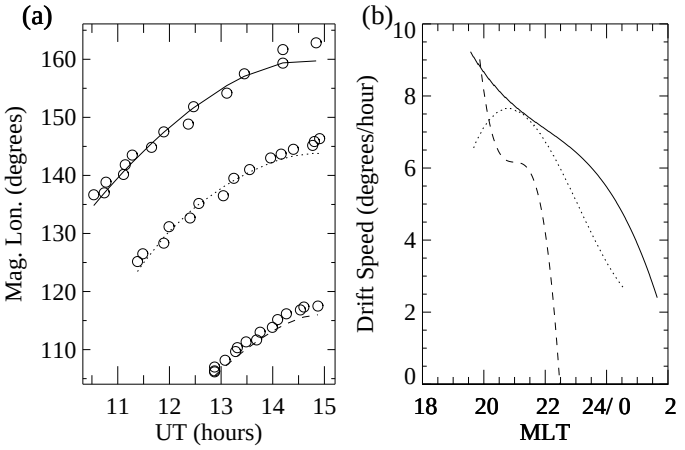

Figure 3. Drift data fitted to determine drift velocity (a) The track of three of the brightness decreases from Figure 2b in UT vs. Mag. Lon., with 4-th degree polynomial fits overlaid. (b) Speed of the brightness depletions in degrees per hour. Solid, dotted, and dashed lines are used to separately indicate each of the three traces from Figure 3a.

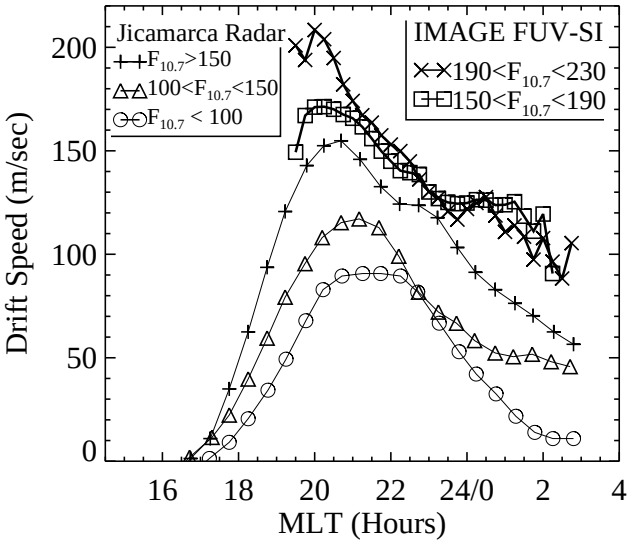

Figure 4. Average plasma drift velocities across the nightside for >40 days in 2002. The eastward velocity of identifiable plasma depletions is determined as shown in Figure 3 for every IMAGE observational period between days 82 and 129, 2002. The data are separated into two ranges of $F_{10.7}$, where the separation of 190 Jy is the mean value for all the observations. Shown for comparison (in 3 bins of $F_{10.7}$) are average data from the Jicamarca radar described by *Fejer et al.* [1991].

on the ground would appear as vertical traces in this display. For reference, the 20 MLT position is indicated with a solid line, decreasing in longitude with time. As in the previous plot , the FUV brightness decreases are obvious, and now clearly demonstrate a drift toward greater longitudes (eastward). What is also clear from the pair of plots in Figure 2 is that the drifts are most rapid at early evening local times, slowing down by a factor of 2 or more by midnight. The first three depletions to pass through the 20 MLT sector are indicated in each panel of Figure 2, as they will now be further analyzed.

To determine the drift speed of individual plasma depletions, the Mag. Lon. and UT of the center of the depletion is determined at 15 points in the keogram, and a least-squares fit to the data is determined, using a 4-th degree polynomial. The derivative of the fitted data is then calculated, giving the fitted instantaneous drift speed of the depletion over the time of observation. The calculated speeds are subequently converted from (Mag. Lon.)/sec to absolute ground speed in m/sec, a correction of up to 15%. This method is applied for the 3 separate depletions indicated in Figure 2and the results shown in Figure 3. Plotted now with UT on the abscissa, the position as a function of time for the 3 depletions is shown in Figure 3a, with the polynomial fits overlaid. The derivatives of the 3 fits are shown in Figure 3b, which show the instantaneous drift speed as a function of MLT. The speeds are greatest in early evening, with values between 6 and 9 degrees/hour in the 20 MLT sector.

This technique is applied to outstanding plasma depletions observed from days 87-129, 2002, and the resulting average drift speeds from 94 samples are shown in Figure 4. The data are actually separated into two groups by the daily 10.7-cm solar flux values ($F_{10.7}$), which serves as a proxy for the solar EUV flux [*Hedin*, 1984]. The median and mean for the dataset are both ∼190 Jy, so that is selected as the separating value, with mean $F_{10.7}$ values of 171 and 208 Jy in the low and high flux bins, respectively. Though both sets show the same general trend with a peak at 20 MLT and decreasing values thereafter, the high flux drift speeds ('x' marks) are ∼40° greater at their peak than the low flux speeds (squares). They remain higher until about 23 MLT.

Also shown in Figure 4 are values for equinox plasma drift speeds determined using the ground-based radar at Jicamarca. These data, taken directly from Figure 7 of *Fejer et al.* [1991], are also organized by $F_{10.7}$, with

average values of 78, 123, and 204 Jy. The trend towards faster drifts with increasing solar EUV flux is apparent in these data as well. Comparing the high flux drift speeds from both data sets, one may note that the overall drift speeds determined from space are 15-20% greater than the radar determined values, with up to a 35% enhancement of peak velocities.

4. Discussion

The difference between the ground- and space-based data presented in Figure 4 is significant. It raises the question of whether the radar and imaging techniques are comparable, as radars do not require large scale plasma inhomogeneities to measure drift speeds. At issue is whether the bubbles are being carried by an ambient plasma that is drifting faster than radars have indicated, or whether the bubbles are drifting faster than the surrounding plasma. There is evidence that both may be important in explaining the difference.

During periods of spread F, the F-region plasma is lofted to higher altitudes where the neutral winds have a higher velocity, contributing to greater plasma drift speeds. Recent work shows that low-latitude plasma bubbles can have a larger eastward velocity than would be expected if one referred to averages determined using the Jicamarca radar [*Kil et al.*, 2000; *Valladares et al.*, 1996]. Secondly, Jicamarca is located at the magnetic equator, and the maximum eastward drifts are more likely to be found at $\pm 8^\circ$ Mag. Lat. [*Aggson et al.*, 1987]. The technique developed here integrates all observations along magnetic meridians between 0 and 30 degrees Mag. Lat., and thereby includes counts from areas not regularly measured by the Jicamarca radar where the ambient plasma may drift eastward more rapidly, regardless of the occurrence of spread F.

The studies by *Kil et al.* [2000] and *de Paula et al.* [2002] reported the observation of plasma bubbles with eastward drift speeds up to 200 m/sec, in agreement with the results presented here, and in both cases reported speeds greater than those reported by Jicamarca under similar conditions (season and solar flux). It is expected, therefore, that observations like those made with SI-13 will also result in drift speeds in excess of the averages determined at the magnetic equator (i.e. away from the anomalies). FUV measurements along the magnetic equator add very little to the measurement of the integrated brightness of the airglow bands.

5. Conclusion

This paper describes the first space-based FUV observations of drifting low-latitude plasma depletions. A technique has been developed to allow for the determination of the drift speed by tracking the depletions. A modulation of the solar $F_{10.7}$ index by 80 Jy in the 5 weeks of observation manifests itself as a 40 m/sec variation in the peak nightside plasma drift speed. Comparing to earlier ground based work on the importance of the solar input on drift speeds, this variation is of the magnitude expected for the given change in solar flux. The local time variation, with a peak speed around 20 MLT and a gradual decrease until midnight, compares well with several ground based studies of low latitude plasma drifts.

Further observations in 2003 and 2004, including direct conjugate observations of the southern arc, will be useful in addressing the question of plasma bubble frequency vs. magnetic activity. Also, the degree of conjugacy of the arcs during equinox conditions will be important for discussions of high-latitude effects on the equatorial ionosphere. Observation of the development of plasma density decreases associated with spread-F and the simultaneous determination of plasma drift speeds across the active evening ionosphere could prove to be a very significant contribution to the mature field of equatorial ionospheric physics.

Acknowledgments. IMAGE FUV analysis is supported by NASA through Southwest Research Institute subcontract number 83820 at the University of California, Berkeley, contract NAS5-96020.

References

Aggson, T. L., N. C. Maynard, F. A. Herrero, H. G. Mayr, L. H. Brace, and M. C. Liebrecht, Geomagnetic equatorial anomaly in zonal plasma flow, *J. Geophys. Res.*, *92*, 311–315, 1987.

Burch, J. L., IMAGE mission overview, *Space Sci. Rev.*, *91*, 1–14, 2000.

Carruthers, G. R., and T. Page, Apollo 16 far ultraviolet imagery of the polar auroras, tropical airglow belts, and general airglow, *J. Geophys. Res.*, *81*, 483–496, 1976.

de Paula, E. R., et al., Ionospheric irregularity zonal velocities over cachoeira paulista, *J. Atmos. Solar-Terr. Phys.*, *64*, 1511–1516, 2002.

Fejer, B. G., E. R. de Paula, S. A. González, and R. F. Woodman, Average vertical and zonal F region plasma drifts over Jicamarca, *J. Geophys. Res.*, *96*, 13,901–13,906, 1991.

Frey, H. U., et al., Summary of quantitative interpretation

of IMAGE far ultraviolet auroral data, *Space Sci. Rev.*, p. in press, 2003.

Hanson, W. B., and R. J. Moffett, Ionization transport effects in the equatorial F region, *J. Geophys. Res.*, *71*, 5559, 1966.

Hedin, A. E., Correlations between thermospheric density and temperature, solar EUV flux, and 10.7-cm flux variations, *J. Geophys. Res.*, *89*, 9828–9834, 1984.

Kelley, M. C., *The Earth's Ionosphere Plasma Physics and Electrodynamics*, Academic Press, Inc., San Diego, 1989.

Kil, H., P. M. Kintner, E. R. de Paula, and I. J. Kantor, Global Positioning System measurements of the ionospheric zonal apparent velocity at Cachoeira Paulista in Brazil, *J. Geophys. Res.*, *105*, 5317–5327, 2000.

Mende, S. B., et al., Far ultraviolet imaging from the IMAGE spacecraft. 1. Systems design, *Space Sci. Rev.*, *91*, 243–270, 2000a.

Mende, S. B., et al., Far ultraviolet imaging from the IMAGE spacecraft. 3. Spectral imaging of Lyman-α and OI 135.6 nm, *Space Sci. Rev.*, *91*, 287–318, 2000b.

Richmond, A. D., Ionospheric electrodynamics using magnetic apex coordinates, *J. Geomagn. Geoelectr.*, *47*, 191–212, 1995.

Sagawa, E., T. Maruyama, T. J. Immel, H. U. Frey, and S. B. Mende, Global view of the nighttime low latitude ionosphere by the 135.6 nm OI observation with IMAGE/FUV, *Geophys. Res. Lett.*, p. submitted, 2003.

Sojka, J. J., Ionospheric physics, *Rev. Geophys.*, *29*, 1166–1186, 1991.

Valladares, C. E., R. Sheehan, S. Basu, H. Kuenzler, and J. Espinoza, The multi-instrumented studies of equatorial thermosphere aeronomy scintillation system: Climatology of zonal drifts, *J. Geophys. Res.*, *101*, 26,839–26,850, 1996.

Weber, E. J., J. Buchau, R. H. Eather, and S. B. Mende, North-south aligned equatorial airglow depletions, *J. Geophys. Res.*, *83*, 712–716, 1978.

T. J. Immel, S. B. Mende, H. U. Frey, L. M. Peticolas, Space Sciences Laboratory, University of California, Berkeley, CA, 94720 (email: immel@ssl.berkeley.edu)

Eiichi Sagawa, Communications Research Laboratory, Tokyo, Japan (email:esagawa@crl.go.jp)

Received February 27, 2003; accepted ? ?, 2003.